Diagenetic alteration of benthic foraminifera from a methane seep site on the Vestnesa Ridge (NW Svalbard margin)

Andrea Schneider[1*], Antoine Crémière[2,1], Giuliana Panieri[1], Aivo Lepland[2,1], Jochen Knies[2,1]

[1] CAGE - Centre for Arctic Gas Hydrate, Environment and Climate, Department of Geosciences, UiT the Arctic University of Norway, 9037 Tromsø, Norway

[2] Geological Survey of Norway, 7491 Trondheim, Norway

* Corresponding author:
Andrea Schneider
Centre for Arctic Gas Hydrate, Environment and Climate
Department of Geosciences
UiT The Arctic University of Norway
Dramsveien 201, NO-9037 Tromsø
andrea.schneider@uit.no

Abstract

Anomalously low $\delta^{13}C$ values in foraminifera calcite tests are due to diagenetic alteration in methane seep sites. Our study applies diagenetically altered fossil benthic foraminifera tests as geochemical tracers in reconstructing past methane seepage episodes at the Vestnesa Ridge offshore NW Svalbard. We combine examinations of the test wall microstructure, mineralogical and stable carbon isotope composition of foraminifera and co-occurring authigenic carbonate nodules. We present a classification of visual and mineralogical characteristics of the exterior and interior wall microstructure of the benthic foraminiferal species *Cassidulina neoteretis* having experienced different degrees of diagenetic alteration during methane seepage. Carbonate nodules comprising high-Mg calcite cement with 13-15 mol % $MgCO_3$ have $\delta^{13}C$ values as low as -32.3 ‰, which is consistent with a methane-derived origin. The visual, mineralogical and stable isotope investigations of *C. neoteretis* indicate a variable degree of diagenetic alteration and show $\delta^{13}C$ values between -0.6 and -16.9 ‰. The negative $\delta^{13}C$ values in benthic foraminifera are largely caused by precipitation of isotopically light methane-derived authigenic carbonate as high-Mg-calcite coatings, whose relative contribution to the bulk foraminifera carbonate is estimated to be up to 58 wt %. Another key finding is the identification a first seepage episode concurrent with Heinrich Event 1 (HE 1), and a second episode at the onset of the Bølling-Allerød period.

Keywords: Foraminifera; methane seepage; authigenic carbonate; diagenesis; stable carbon isotopes

Highlights

- Diagenetically altered foraminifera can be used as a tracer for methane seepage.
- The degree of diagenetic alteration displays variable methane seepage intensity.
- Diagenetically altered foraminifera report two seepage episodes (HE1; Bølling-Allerød).
- Seepage during HE1 lasted longer than previously constrained.

1 Introduction

A large amount of methane is trapped as methane hydrates and free gas reservoirs in continental margin sediments worldwide that can be released into the water column and atmosphere during future global climate warming. Assessment of the climatic effects of such release demands the development of better tracers to improve our understanding of the intensity and timing of natural past methane seepage.

A striking feature in the geochemical environment of methane seeps is the presence of methane-derived ^{13}C-depleted dissolved inorganic carbon (DIC). In sediments exposed to methane seepage, a microbial consortium consisting of archaea and sulphate-reducing bacteria mediates anaerobic oxidation of methane (AOM) (Boetius et al., 2000). The bicarbonate (HCO_3^-) ions produced during AOM react with calcium and magnesium ions present in the pore water and precipitate as methane-derived authigenic carbonate (MDAC) that are commonly strongly ^{13}C-depleted (Aloisi et al., 2000; Bayon et al., 2007; Crémière et al., 2016, 2012; Greinert et al., 2001; Naehr et al., 2007).

The carbon isotope composition of foraminiferal test calcite preserved in the stratigraphic record has long been recognized to reflect changes in paleo-environmental conditions. In a marine environment unaffected by methane seepage, $\delta^{13}C$ values measured in the calcitic tests of benthic foraminifera range between 0 and -1.9 ‰ depending on the species (Wollenburg et al. 2001; Rathburn et al. 2003; Hill et al. 2004; Mackensen et al. 2006; Panieri and Sen Gupta, 2008). At seafloor methane seeps, episodic negative excursions in the $\delta^{13}C$ signature of foraminifera are frequently observed (e.g. Wefer et al., 1994; Kennett and Stott, 1991; Stott, 2002; Thomas, 2002). In many cases, living foraminifera sampled from seep locations show slightly negative $\delta^{13}C$ values (as low as -5.6 ‰) in calcite tests (Hill et al., 2004; Sen Gupta et al., 1997), while the $\delta^{13}C$ value of fossil test calcite can be significantly more negative (less than -5.6 ‰) (Consolaro et al., 2015; Hill et al., 2004; Millo et al., 2005; Martin et al., 2010, 2007; Panieri, 2006; Panieri et al., 2014; Torres, 2003). Rapidly expanding knowledge on the geochemical conditions of seafloor methane seeps has contributed to developing an explanation for those foraminiferal $\delta^{13}C$ excursions, and suggests their application as proxies for reconstructing past methane seepage (e.g. Wefer et al., 1994; Kennett and Stott, 1991; Stott, 2002; Thomas, 2002).

Opinions about the origin of extraordinarily negative $\delta^{13}C$ values recorded in foraminifera are divergent. Several studies address the origin of the $\delta^{13}C$ signatures by comparing the $\delta^{13}C$ of DIC in bottom and interstitial water with the $\delta^{13}C$ of test calcite from living and dead specimens (Herguera et al., 2014; Hill et al., 2004; Mackensen et al., 2006; Martin et al., 2010; Rathburn et al., 2000; Torres, 2003). For instance, Herguera et al. (2014) compared $\delta^{13}C$ signatures of porewater DIC with the $\delta^{13}C$ signature of living benthic foraminifera and demonstrated that methane-derived DIC from porewater is not directly incorporated during the primary biomineralization of the test. Whereas a recent publication by Wollenburg et al. (2015) using novel culturing techniques resembling deep-sea conditions with injections of methane supports the idea that the uptake of methane-derived carbon during biomineralization is reflected in the test $\delta^{13}C$ composition of benthic foraminifera. Despite controversial results, one explanation for slightly negative $\delta^{13}C$ values of the test calcite (as low as -5.6 ‰) is that foraminifera incorporate methane-derived DIC from the ambient water during the biomineralization (Panieri et al., 2014; Panieri and Sen Gupta, 2008; Rathburn et al., 2003; Sen Gupta et al. 1997). An alternative explanation for the slightly negative $\delta^{13}C$ values in benthic foraminifera include abundant chemosynthetic microbial nutrition sources carrying ^{13}C-depleted carbon in their body tissue (Rathburn et al., 2003; Torres, 2003; Hill et al., 2004; Panieri, 2006; Panieri & Sen Gupta 2008).

After the death of the organisms and the burial of their tests in the sediment, diagenetic alteration of both benthic and planktic foraminiferal tests through the precipitation of MDAC crystals may cumulatively add a second phase of carbonate with a strongly negative $\delta^{13}C$ value. Thus, MDAC precipitation can overprint the isotope signal of the pristine biogenic test leading to $\delta^{13}C$ values as low as -10 ‰ and below (Torres 2003; Millo et al. 2005; Martin et al. 2007; Consolaro et al. 2015; Panieri et al. 2014, 2016a). Visible changes in the foraminifera test microstructure and wall surface texture due to diagenetic alteration have been described on complete tests and polished wall sections by Edgar et al. (2013), Sexton and Wilson (2009), Regenberg et al. (2007) and Sexton et al. (2006) for planktonic foraminifera in the context of paleoceanographic reconstructions. Sexton et al. (2006) introduce the term “glassy” for translucent tests resembling the appearance of living foraminifera, and “frosty” for tests having their interior and exterior walls extensively coated with diagenetic minerals.

In order to unravel the contribution of MDAC to the $\delta^{13}C$ signal in foraminifera, we investigate the test wall microstructure, the mineralogical and stable isotope composition from benthic foraminifera and carbonate nodules using light microscopy, Scanning Electron Microscopy (SEM) coupled with Energy Dispersive X-ray Spectrometry (EDS) and mass spectrometry. Based on visual and geochemical investigations, we develop a framework of criteria to identify different states of diagenetic alteration. Furthermore, our mass balance approach allows the estimation of the relative contribution of MDAC in the bulk isotope signal of fossil foraminifera. Our study is the first detailed investigation of a distinct

seepage episode that occurred for about 1 000 years between 17 700 and 16 680 cal years BP concurrent with HE 1 (Bond et al. 1993) and was earlier identified by Ambrose et al. (2015) based on findings of chemosynthetic bivalves. We seek to systematically classify the test wall microstructure of diagenetically altered benthic foraminifera, investigate the MDAC contribution to the foraminifera test $\delta^{13}C$ value, and evaluate the suitability of diagenetically altered foraminifera for tracing paleo-methane seepage timing and intensity.

2 Setting of the study site

The Vestnesa Ridge is an elongated sediment drift located at 79° N at the NW Svalbard continental margin in the eastern Fram Strait (Figure 1). The Molloy Deep bounds the Vestnesa Ridge in the west and the Molloy Transform Fault and the Knipovich Ridge in the south (Plaza-Faverola et al., 2015; Winkelmann et al., 2008). The Vestnesa Ridge in about 1200 m water depth is approximately 100 km long and bends SE–NW to E–W. Its sediments reach a thickness of > 2 km (Eiken and Hinz, 1993), resting on < 20 Ma old oceanic crust (Hustoft et al., 2009) that is part of an ultraslow spreading ridge (Johnson et al., 2015). Sediments at the NW Svalbard continental margin have been divided into three seismostratigraphic units including syn-rift and post-rift deposits (YP-1), contourites (YP-2) and glaciomarine contourites and turbidites (YP-3) (Mattingsdal et al., 2014). The youngest sediments of Late Pleistocene and Holocene age at the Vestnesa Ridge are composed of silty contourites, turbidites and hemipelagites with abundant ice rafted debris (Howe et al., 2008).

The crest of the Vestnesa Ridge is pierced by active and inactive pockmarks that are formed in areas of highly localized seepage of fluids in unconsolidated fine-grained sediments (Vogt et al., 1994; Judd and Hovland, 2007). Pockmarks on the Vestnesa Ridge vary in size and can be as large as 700 m in diameter (Bünz et al., 2012).

The Vestnesa Ridge hosts a subsurface gas hydrate system with significant amounts of trapped gas that is susceptible to seepage in response to tectonic stress. Seismic studies indicate that multiple seepage episodes have occurred during the last 2.7 Ma being closely linked to fault reactivation and fracturing (Plaza-Faverola et al., 2015).

A seismic Bottom Simulating Reflector (BSR) located at 200 ms bsf TWT (~160-180 m bsf, below sea floor) suggests the presence of free gas and methane hydrate in the pore space of the deeper sediment layers (Petersen et al. 2010; Bünz et al. 2012). In seismic studies, vertical fluid flow conduits were observed to cross cut the bedded sediment layers and bypass the BSR. Those conduits connect the pockmarks at the seafloor with the methane reservoir, allow the gas to migrate vertically, and finally escape into the water column. Numerous up to 900 m high gas flares were observed by Smith et al.

(2014) in recent times. The geochemical measurements of gas from hydrates collected at the Vestnesa Ridge reveal the thermogenic origin of the gas (Smith et al., 2014).

3 Methodology

3.1 Core collection and non-destructive analyses

During the CAGE HH-13 cruise using the research vessel R/V Helmer Hanssen (The Arctic University of Tromsø), gravity core HH-13-203 (79°00.14N, 06°55.68E, 300 cm sediment recovery, 11 cm core diameter) was collected from an active pockmark with a gas flare in 1210 m water depth (Mienert, 2013). After recovery, the core was cut into 100 cm sections and kept cool at 5°C. At the Department of Geology at The Arctic University of Norway in Tromsø, the cores were split longitudinally, described visually, photographed (Jai L-107CC 3 CCD RGB Line Scan Camera) and X-ray-scanned (Geotek MSCL-XR 3.0). The presented element-geochemical data were acquired with an Avaatech XRF Core Scanner at 1 cm steps using the following settings: down-core slit size: 10 mm; cross-core slit size: 12 mm; 10 kV; 1000 µA; no filter; and 10 seconds measuring time. The raw data were subsequently processed with the software WinAxil. We show here the calcium (Ca) counts normalized to Aluminium (Al) for the purpose of identifying carbonate-rich intervals in the sediment core (Richter et al., 2006).

3.2 Visual investigations of foraminifera tests and carbonate nodules

Sediment samples for micropalaeontological and stable isotope analysis were collected typically at 10 cm intervals in 1 cm thick slices and at higher spatial resolution in the depth interval from 220 to 270 cm (Table 1). The samples were weighed and wet-sieved (mesh sizes 63 µm; 100 µm; 1 mm) after freeze-drying. The sieve residues were dried at 40°C and subsequently investigated using light microscopes. About 15-28 specimens of the benthic foraminifera species *C. neoteretis* (Seidenkrantz, 1995) were picked for bulk isotope measurements from the dry residue of the >100 µm size fraction. This species was selected since it is most abundant throughout the core, and it also is abundant in the Arctic Ocean. Unbroken tests of *C. neoteretis* were picked for visual inspection and photographed using a Leica DFC 450 digital camera mounted on a Leica Z16 Apo light microscope. About 15 images with different focal plains of the three-dimensional test were stacked using Zeiss Helicon Focus software and described adopting the terminology developed by Edgar et al. (2013), Sexton and Wilson (2009) and Sexton et al. (2006).

For SEM analyses of selected samples, five complete foraminifera specimens were placed on adhesive tape in a circular 25 mm diameter mold, mounted using Struers Epofix, and polished to expose cross-sections through the tests. This allows studying the microstructure of the test walls and the interior of

the chambers. After polishing, the samples were washed with MilliQ water for 10 minutes in an ultrasonic bath. Complete specimens and polished sections of foraminifera were examined with a SEM Hitachi Tabletop Microscope TM-3000 and a SEM Carl Zeiss LEO 1450VP.

The state of preservation of *C. neoteretis,* which has a hyaline calcareous finely perforated wall, was characterized by investigating 5-30 specimens using light microscopy and up to five specimens with SEM imagery of test microstructures, and combined with geochemical analyses. The microstructure of the whole test, its exterior wall texture, wall cross section, the chamber interior and pore areas are best viewed in high-resolution SEM images. Subsequently, the same (up to five) imaged specimens were analysed by EDS to assess the elemental composition of the test and secondary precipitates. The uncalibrated EDS measurements do not provide an absolute quantification of the elemental composition of the studied material, but allow for a semi-quantitative assessment. When investigating the secondary precipitates, we focus on its relative Mg-content being indicative of methane-induced diagenetic alteration (Aloisi et al., 2000).

In order to systematically describe our observations, we introduce an array of criteria for the test microstructure and elemental composition in order to distinguish the degree of diagenetic alteration. Firstly, for the exterior wall we considered surface characteristics such as reflectance, transparency, colour, and ornamentation (aspect of pores); secondly, for the Interior wall we considered the surface characteristics, and the presence of secondary minerals (high-Mg calcite).

The core interval between 170 to 280 cm contains carbonate nodules composed by carbonate cemented sediments (Table 1). We crushed the nodules in order to expose their structure and investigated their visual appearance using SEM.

3.3 Stable isotope analyses

Stable carbon ($\delta^{13}C$) and oxygen ($\delta^{18}O$) isotope analyses of 20 *C. neoteretis* samples, consisting of 15 to 28 tests, and 11 carbonate nodules were performed using a ThermoFinnigan MAT252 mass spectrometer coupled to a CarboKiel-II carbonate preparation device at the Serveis Cientifico-Técnics of the University in Barcelona, Spain. Analytical precision was estimated to be better than 0.03 ‰ for carbon and 0.08 ‰ for oxygen by measuring the certified standard NBS-19. We report all isotope results in standard delta notation relative to Vienna Pee Dee Belemnite (VPDB).

3.4 Mineralogy and petrography

We studied the elemental composition of complete specimens and polished cross-sections of *C. neoteretis* using a SEM Hitachi Tabletop Microscope TM-3000 equipped with a Bruker Quantax 70

Energy Dispersive X-ray Spectrometer. Element mapping was performed for a time interval of 360 seconds.

On the same carbonate nodule samples that were used for determining stable isotope ratios (Table 1), we performed XRD analyses of unoriented samples using a Bruker D8 Advance diffractometer (Cu K_α radiation in 3-75° 2θ range). The quantitative mineralogical composition of the carbonate phases were interpreted and modeled by using the Rietveld algorithm-based code Topas-4 by Bruker. Following a displacement correction of the spectrum made on the main quartz peak, the displacement of calcite d_{104} was used to estimate the $MgCO_3$ mol % (Goldsmith and Graf, 1958).

4 Results

4.1 Lithology and chronology

A detailed sedimentological description and the chronological framework of the gravity core HH-13-203 is published by Ambrose et al. (2015), and here we report its main characteristics. The core recovered 300 cm of Late Pleistocene and Early Holocene sediments composed of homogeneous dark grey clay with mm-sized carbonate nodules, shell fragments, and isolated clasts (Figure 2A). In the top 10 cm of the core, diatoms (*Coscinodiscus* spp.) are abundant, belonging to a chronostratigraphic marker horizon on the west Svalbard slope dated to 10 100 ± 150 to 9 840 ± 200 cal years BP (TP 2 and 3 in Jessen et al., 2010). Gravel-sized clasts of variable lithology are present in the intervals from 20 to 100 cm and from 210 to 230 cm. The upper contact of a clast-rich layer (210 cm) to homogeneous mud (172-210 cm) corresponds to a clast rich layer in Jessen et al. (2010), dated to 14 780 ± 220 cal years BP (TP 6) while the base of core HH-13-203 (290.5 cm) is dated to 21 031 cal years BP (Ambrose et al., 2015). In the stratigraphic interval between 236 and 268 cm, dated to 16 680 cal years BP near the top of the interval, complete valves and shell fragments of juvenile and mature bivalves and gastropods identified as members of a chemosynthesis-based macrofaunal community (hereafter named shell bed).

High Ca/Al ratios occur in intervals with carbonate nodules (220-280 cm) and between 170-180 cm. The nodules occur at the stratigraphic position of the shell bed, but also above and below it (Figure 2A). The present-day sulphate-methane transition zone (SMTZ) is located at 100-140 cm (Hong et al., 2016). The nodules are composed of irregular 5-10 µm sized carbonate crystals with disseminated pyrite (Figure 3 A) cementing detrital grains (Figure 3 C; D). Despite the solid appearance of the carbonate nodules, porosity was relatively high (Figure 3 B). Our XRD analyses indicate that the carbonate phase in the nodules is high-Mg calcite with 13-15 mol % of Mg. The $\delta^{13}C$ values of the carbonate nodules (Table 1) range between -32.4 ‰ (246 cm) and -11.6 ‰ (280.5 cm) while the $\delta^{18}O$ values from 5.3 ‰ (280.5 cm) to 6.7 ‰ (246 cm).

4.2 State of preservation and chemical composition of benthic foraminifera tests

The preservation of foraminiferal tests in core HH-13-203 is generally good in sediment intervals from 0 to 160 cm (tentative age: Early Holocene), at 200 cm (tentative age: Bølling-Allerød) and below 280 cm (tentative age: post-LGM). The preservation varies from 160 to 190 cm, in the shell bed (236 to 268 cm, 17 to 16 cal kyr BP), and above and below it (220 to 280 cm, tentative age: equivalent to HE 1). Based on our criteria of the test microstructure, we describe pristine and three stages of diagenetic alteration of the tests of *C. neoteretis* (Figs. 4, 5). At the current position of the SMTZ *C. neoteretis* is absent.

4.2.1 Pristine foraminifera

Well-preserved pristine *C. neoteretis* tests from stratigraphic intervals from 0 to 160 cm, at 200 cm and below 280 cm resemble modern living foraminifera tests (Figs. 4, 5). The tests are optically smooth with high reflectance and transparency. The "glassy" (Sexton et al., 2006) appearance makes morphological features such as chambers, sutures and even pores easy to observe when using light microscopy. SEM imagery does not reveal foreign grains or crystals on exterior and interior walls, pores are unplugged, and wall cross sections are homogeneous with a well-defined outline. The tests are composed of biogenic low Mg-calcite; anomalous amounts of high-Mg calcite are not observed. In most foraminifera species, the original magnesium amount of the seawater is heavily reduced during biomineralization of the tests, resulting in a Mg content as low as 0.2 $MgCO_3$ (Bentov and Erez, 2006; Blackmon and Todd, 1959).

4.2.2 Minor diagenetic alteration

Tests having experienced minor diagenetic alteration cannot be distinguished using light microscopy exclusively. The exterior walls of those tests are glassy, but exhibit decreased reflectance and transparency (Figs. 4, 5). The tests are white in colour or translucent, morphological features are well visible, and pores are unplugged. In contrast to pristine tests, SEM-EDS data reveal a fine-grained approximately 1-3 µm thick patina of high-Mg calcite crystals on the interior and/or exterior test walls.

4.2.3 Moderate diagenetic alteration

Foraminiferal tests with moderate diagenetic alteration appear white or yellow in the light microscope. The tests have lost their optically smooth surface texture, transparency and reflectance. Instead, SEM-EDS observations reveal a pervasive coating with high-Mg calcite crystals covering the interior and exterior walls (Figs. 4, 5). The mineral precipitation generates a "frosty" wall texture (Sexton et al.,

2006). Pores and pore rims on interior walls remain free of diagenetic precipitates. The visibility of micro morphological features (sharply outlined sutures and pores) is deteriorating while wall cross sections remain homogeneous and solid.

4.2.4 Major diagenetic alteration

In the light microscope, foraminiferal tests having experienced major diagenetic alteration appear frosty, with low reflectance and transparency, and yellow to dark brown in colour. Sometimes they can be dark grey or black.

SEM-EDS studies demonstrate that high-Mg calcite crystals cover the exterior and interior walls forming a solid crust (Figs. 4, 5). The crusts on the interior walls are up to 10 µm thick and appear slightly darker on electron backscatter images due to lower backscatter response of high-Mg calcite compared to biogenic calcite. Observations of high-Mg calcite crystals entirely plugging the pores and filling the chambers are limited to the stage of major diagenetic alteration of the benthic foraminiferal tests. We observe that the Mg-content of the precipitate due to the cumulatively added amount of secondary minerals increases with stronger diagenetic alteration (Figure 5).

4.3 Stable isotope composition of foraminifera

Our results reveal that pristine (glassy) tests of *C. neoteretis* exhibit $\delta^{13}C$ values ranging from -0.6 to -3.3 ‰ (Table 1). In contrast, foraminiferal tests with different diagenetic alteration stages occurring in the same sample in the intervals between 160 to 190 cm and 220 to 280 cm have $\delta^{13}C$ values ranging from -4.5 ‰ (230 cm) to -16.9 ‰ (180 cm, Figure 2, Table 1). In the shell bed (236 to 268 cm) where tests show primarily major diagenetic alteration, $\delta^{13}C$ values range from -7.7 ‰ (270 cm) to -10.6 ‰ (240 cm, Figure 2, Table 1).

The oxygen isotope values are less variable ranging from 4.3 ‰ to 5.3 ‰ and exhibit a slight tendency of enrichment in ^{18}O in the stratigraphic interval with diagenetic alteration (Figure 2, Table 1).

5 Discussion

5.1 MDAC precipitation on benthic foraminiferal tests

A $\delta^{13}C$ range between 0 and -1 ‰ is considered to represent normal marine conditions in *C. neoteretis* tests from the northern Barents Sea (0 to -1 ‰, Wollenburg et al., 2001) and a control site at the Håkon Mosby Mud Volcano (-1.15 ‰, Mackensen et al., 2006). In our $\delta^{13}C$ record, the majority of the $\delta^{13}C$ values from *C. neoteretis* (Table 1) deviate from values expected in a normal marine environment. As

previously observed, the foraminifera can incorporate ^{13}C-depleted methane-influenced DIC while metabolically active (Hill et al., 2004; Panieri and Sen Gupta, 2008) but when the $\delta^{13}C$ values of foraminifera tests are lower than -5.6 ‰, like in our study, this appears unlikely. We argue that methane seepage from the Vestnesa Ridge caused diagenetic alteration due to MDAC precipitation on foraminifera tests, leading to strongly negative $\delta^{13}C$ values (as low as -16.9 ‰).

The $\delta^{13}C$ values of the carbonate nodules found in the shell bed that formed during a seepage episode support that they originate from AOM. Mg-rich carbonates having low $\delta^{13}C$ values are known to dominate in cold-seep settings and exhibit distinctive chemical and lithologic characteristics (e.g. Aloisi et al., 2000; Bayon et al., 2007; Greinert et al., 2001; Naehr et al., 2007). For example, the negative $\delta^{13}C$ values of the carbonate nodules studied here are consistent with other $\delta^{13}C$ values measured in 3 000 years old authigenic carbonate crusts found offshore western Svalbard (Berndt et al., 2014), MDAC from the Marmara Sea (Crémière et al., 2013), the Black Sea (Mazzini et al., 2004), the Gulf of Mexico (Formolo et al., 2004), Monterey Bay (Stakes et al., 1999), and the Cascadia margin (Bohrmann et al., 1998; Greinert et al., 2001).

The visual appearance and mineralogical composition of MDAC nodules and the secondary mineral precipitates on foraminifera are identical, suggesting the precipitation of MDAC crystals on the test. A recent paper (Panieri et al., 2016b) found that foraminiferal calcite and authigenic Mg-calcite overgrowths have identical crystal lattice fringes, meaning they are structurally identical, such that foraminifera serve as preferred nucleation templates for authigenic Mg-calcite. Foraminifera in sediment intervals between 160 and 280 cm have $\delta^{13}C$ values as low as -16.9 ‰ (Table 1). Strongly negative $\delta^{13}C$ values in the range of -7 to -9 ‰ (Torres, 2003), beyond -12 ‰ (Hill et al., 2004), -17 to -19.5 ‰ (Millo et al., 2005), -9.04 to -25.74 ‰ (Panieri et al., 2009), -15 to -30 ‰ (Panieri et al. 2016a), and -29.8 to -35.7 ‰ (Martin et al., 2010) have also been interpreted to reflect diagenetic alteration by precipitation of ^{13}C-depleted MDAC crystals on foraminifera tests. This is also consistent with two earlier studies from the Vestnesa Ridge performed by Panieri et al. (2014) and Consolaro et al. (2015). Comparing the $\delta^{18}O$ and $\delta^{13}C$ compositions of the carbonate nodules and the benthic foraminifera (Figure 6) reveals a clustering of values into three groups with little overlap. The $\delta^{13}C$ values distinguish unaltered foraminifera tests (cluster A, $\delta^{13}C \geq$ -3.2 ‰, $\delta^{18}O$ from 4.3 to 4.9 ‰), diagenetically altered foraminifera tests (cluster B, $\delta^{13}C$ from -4.5 to -16.9 ‰, $\delta^{18}O$ from 4.8 to 5.2 ‰), and MDAC nodules (cluster C, $\delta^{13}C$ from -11.6 to -32.3 ‰, $\delta^{18}O$ from 5.3 to 6.7 ‰). The intermediate position of cluster B suggests a shift of the pristine tests towards more negative $\delta^{13}C$ values that only MDAC precipitation can explain.

However, one carbonate nodule, found at 280.5 cm, falls outside the observed isotopic range of nodules, but shows close proximity to foraminiferal calcite. We interpret this nodule as consisting

mainly of biogenic carbonate from microfossils or a bivalve shell fragment that was masked by MDAC precipitate, and was therefore not identified as biogenic material.

5.2 Foraminiferal tests as a template for carbonate precipitation

In methane seeps, benthic foraminifera may experience passively secondary overgrowth by MDAC. Donners et al. (2002) point out that the formation of biominerals and secondary carbonate growth is controlled by a template offering surface properties such as a suitable molecular structure. Thus, pristine biogenic test calcite walls may favour the precipitation of a secondary carbonate phase. On *C. neoteretis* tests, the authigenic high-Mg calcite crystals precipitate on the interior and exterior walls until they cover the entire test, initially avoiding the pore areas (Figure 7). Carbonate coating, particularly in the pore area of interior walls, may play an important role in understanding the formation of the carbonate overgrowths on benthic foraminifera. Initially, pores themselves and the surrounding pore mounds remain unaffected by crystal growth (Figure 7, A-E) until the tests reach the stage of major diagenetic alteration when authigenic carbonate is encrusting the walls and nearly completely filling the chambers (Figure 7, F). Therefore, our observations show that foraminifera tests act as nucleation templates for authigenic carbonate crystals, as previously suggested by Panieri et al. (2016a) and finally proved by Panieri et al. (2016b). This assertion does not exclude MDAC formation occurring also around other precipitation nuclei with a different chemical composition and surface structure, but suggests the importance of calcitic microfossils as crystallization template. However, we cannot fully exclude selective removal of secondary crystals during sonicating.

5.3 Quantification of MDAC overgrowth on benthic foraminifera

Stable carbon isotope measurements performed on diagenetically altered foraminifera comprise a signal composed of two components: 1) the biogenic calcite of the pristine foraminifera, and 2) the secondary MDAC precipitate. In order to determine the amount of MDAC on foraminifera, the two components need to be evaluated separately.

Chemical cleaning procedures as suggested by Boyle and Rosenthal (1996) and developed onwards by Pena et al. (2005) are one possibility to separate the components. The method aims at eliminating contaminant phases and mineral coatings from the foraminifera, but it is difficult to control the exact amount of authigenic carbonate being removed (Panieri et al., 2008; Consolaro et al., 2015). Furthermore, the cleaning procedure cannot remove authigenic carbonate crystals that might be intergrown with the pristine test material (Panieri et al., 2016b), and it is possible that biogenic calcite of the pristine foraminifera may also be attacked.

In order to estimate the relative contribution of MDAC in the bulk isotope signal of the foraminifera, we apply a mass-balance approach. We assume that the bulk carbon isotope measurement of

foraminifera is a result of mixing two end-member components; the pristine foraminifera tests and the MDAC represented by carbonate nodules. This method allows estimating the relative amount of MDAC overgrowth ($weight_{MDAC}$ in %) on the pristine bulk foraminifera and is expressed by the following equation:

$$weight_{MDAC} = (\delta^{13}C_{bulk\text{-}foram} - \delta^{13}C_{pristine\text{-}foram}) / (\delta^{13}C_{MDAC} - \delta^{13}C_{pristine\text{-}foram}) \times 100 \quad (1)$$

where $\delta^{13}C_{bulk\text{-}foram}$ corresponds to the $\delta^{13}C$ measured from 15 to 28 individual *C. neoteretis* tests. $\delta^{13}C_{pristine\text{-}foram}$ represents the assumed $\delta^{13}C$ of pristine foraminifera that is -1 ‰ (Wollenburg et al. (2001). To account for possible incorporation of methane-influenced DIC in original test, we include a second scenario with an initial test calcite composition of -2.8 ‰.This value is the most negative value measured in dead *C. neoteretis* tests at the Håkon Mosby Mud Volcano (Mackensen et al., 2006). The $\delta^{13}C_{MDAC}$ (-28.5 ± 2.2 ‰) is an average of 11 nodule samples measured here.

The results of the isotope mass balance indicate a highly variable amount of authigenic contribution to the foraminiferal carbon isotope signal (Figure 2B, Table 1). Maximum MDAC contribution to the $\delta^{13}C$ signal coincides with sediment intervals with high Ca-content due to the presence of MDAC nodules or bivalve shells, and sediment intervals with diagenetically altered benthic foraminifera. In the shell bed interval, the authigenic component in the $\delta^{13}C$ signal ranges from 19 to 35 wt %, and from 11 to 58 wt % in the interval between 160 and 190 cm, respectively. The highest contribution of MDAC carbon in the bulk isotope signal (55-58 wt %) has been identified at 180 cm, coinciding with the most negative $\delta^{13}C$ value was measured in foraminifera (-16.9 ‰).

5.4 Late Pleistocene and Early Holocene methane seepage at the Vestnesa Ridge

5.4.1 Episodes and timing

Assessing the state of preservation of fossil benthic foraminifera through targeting their test microstructure, mineralogical and stable isotope composition gives a valuable indication about the exposure of the microfossils to methane seepage. In sediment core HH-13-203 from an active pockmark with a gas flare observed on the crest of the Vestnesa Ridge, diagenetically altered benthic foraminifera identify two methane seepage episodes (Figure 2, Table 1), separated by an interval lacking signs of diagenesis (200 cm, well preserved *C. neoteretis* with a $\delta^{13}C$ of -3.25 ‰).

In-situ occurring chemosynthetic Vesicomyidae bivalves document a first seepage episode persisting for about 1 000 years between 17 700 and 16 680 cal years BP (Ambrose et al. 2015), concurrent with HE 1 (Bond et al. 1993). MDAC-cemented bivalves dated to 17 789 ± 182 cal years BP have also been described from a nearby core location by Sztybor and Rasmussen (2016) most likely belonging to the

same faunal community and seepage episode based on the corresponding sediment stratigraphy, species composition, and age. Vesicomyidae are known to colonize hydrothermal vents and hydrocarbon seeps with intermediate methane flux where they live partially burrowed at the sediment surface and rely on sulphide-reducing endosymbiotic bacteria for nutrition (Krylova and Sahling, 2010; Taylor and Glover, 2010; Sahling et al., 2002). The shell bed evolved at the Vestnesa Ridge during a seepage episode most likely associated with tectonic activity and subsequent release of methane-rich fluids (Ambrose et al. 2015; Plaza-Faverola et al., 2015). Findings of diagenetically altered *C. neoteretis* tests and MDAC nodules in the sediment interval between 220 and 280 cm are clearly exceeding the stratigraphic range of the shell bed and the occurrence of MDAC nodules (Figure 2). The seepage episode preserved in diagenetically altered foraminifera and MDAC nodules suggests the termination of the seepage episode was later than previously documented by solely presence of the shell bed. Compared to similar records in north-west Svalbard (Consolaro et al., 2015; Panieri et al., 2014), our dataset may document the longest methane seepage episode on the Vestnesa Ridge during the Late Pleistocene and Early Holocene exceeding 1 000 years.

A second seepage episode (160.5 to 190.5 cm) is recorded in sediments younger than 14 780 cal years BP (Jessen et al., 2010), coeval with the onset of the Bølling-Allerød period (Deschamps et al., 2012; Lucchi et al., 2015). This finding corresponds to seepage episodes identified by Consolaro et al. (2015; CIE I), Panieri et al. (2014; MEE 4), and Sztybor and Rasmussen (2016) in the nearby area, and may suggest a regional event. Consolaro et al. (2015) discuss increased seismicity in response to rapid melting of the Svalbard-Barents Ice sheet during the Bølling Interstadial, while Sztybor and Rasmussen (2016) suggest an increase in bottom water temperature during HE 1 may have led to enhanced methane flux at the beginning of the Bølling-Allerød Interstadial.

5.4.2 Seepage intensity

The presence or absence of benthic chemosynthetic macrofauna, cm-sized MDAC nodules and diagenetically altered benthic foraminifera may suggest variable seepage intensity. Methane seeps hosting benthic macrofaunal assemblages show variations in biomass and species composition according to fluid flow regime and faunal community age (Bowden et al., 2013; Levin et al., 2016). In particular, fluid flow intensity can be highly variable from diffusive to advective transports at rates of a few millimetres to several hundreds of cm per year (Torres et al., 2002), likely determining supply of reduced sulphur and carbon to benthic chemosynthetic organisms. Initial stages of methane seepage are characterized by intense fluid flux supporting the establishment of microbial communities, subsequently allowing larger chemosynthetic organisms with a substantial biomass to colonize the seep site (Levin et al., 2016). Shell beds are interpreted as characteristic for intermediate to intense fluid flux with high chemical supply over time scales of decades to centuries (Callender and Powell,

2000; Kiel, 2010; Bowden et al., 2013; Levin et al., 2016). Thus, the shell bed present in core HH-13-203 indicates that the organisms were supported by strong fluid flux from the Vestnesa Ridge over approximately 1 000 years (Ambrose et al. 2015), causing major diagenetic alteration on foraminifera tests.

In contrast, less intense fluid flow being insufficient to support macrofaunal assemblages could still have enabled foraminifera to record an emission episode through the uptake of ^{13}C-depleted nutrition sources, and/or the precipitation of MDAC. We consider the seepage-triggered formation of MDAC nodules and diagenetic alteration of foraminifera to occur in shallow sub-surface sediments (cm to dm scale) shortly post-dating the sediment deposition. Thus, MDAC nodules and diagenetically altered foraminifera may document a decline in seepage intensity causing the shell bed organisms to vanish. Although no MDAC nodules or chemosynthetic macrofauna occur in the second seepage episode, we attribute the peak values in Ca/Al content and the record's most negative $\delta^{13}C$ value in *C. neoteretis* (-16.9 ‰ at 180.5 cm) may represent a seepage episode with a short-lived but high-intensity seepage pulse, creating this negative $\delta^{13}C$ value.

6 Conclusions

Our results reveal that:

- The mineralogical and stable isotope composition identifies MDAC crystals that precipitated on exterior and interior test walls of the benthic foraminifera species *C. neoteretis* cause the main diagenetic alteration. Based on our observations of the test wall microstructure and mineralogical composition of *C. neoteretis* tests, we propose a classification of the benthic foraminiferal taphonomy that characterizes the exposure of foraminifera to variable methane seepage intensity.
- The large authigenic component in the foraminifera $\delta^{13}C$ signal strongly suggests that MDAC precipitates rather than pristine foraminifera act as geochemical proxy of paleo-methane seepage. The relative contribution of MDAC in the bulk isotopic signal can be as high as 58 wt %. In contrast, the incorporation of isotopically negative carbon from ambient water and nutrition sources during primary biomineralization may have had a minor impact on the $\delta^{13}C$ signature.
- Diagenetic alteration of benthic foraminifera is capable of refining methane seepage reconstructions. In this study, diagenetically altered benthic foraminifera suggest seepage was longer than previously constrained by bivalves in sediment gravity core HH-13-203 and exceeded HE 1. We identified a second less intense seepage episode during the onset of the

Bølling-Allerød period. This is consistent with other studies along the Vestnesa Ridge, suggesting a regional event.

In methane seeps where the precipitation of MDAC is common, testing the status of preservation and diagenetic alteration of fossils prior to geochemical analyses is of crucial significance. Visual analyses of whole tests are insufficient since interior structures and finely sculptured features on a micrometre scale may be overlooked. However, studying the microstructure and geochemical composition of diagenetically altered foraminifera allowed refining a geochemical tracer for identifying past methane seepage episodes in sedimentary records where carbonate concretions or chemosynthesis based bivalve communities might be rare or absent.

7 Acknowledgements

The Norwegian Research Council funded this research through the Centre for Arctic Gas Hydrate, Environment and Climate [grant number 223259] and the NORCRUST project [grant number 255150]. The sediment core was collected during the CAGE-2013 cruise which was lead by Jürgen Mienert. We thank the captain, crewmembers and scientific team of *R/V Helmer Hanssen* for their great contribution. We are indebted to Matthias Forwick for the XRF data support and valuable discussions on the dataset with Joel Johnson. AS was supported by a travel grant through the Norwegian Research School in Climate Dynamics (ResClim). The authors thank Joachim Schönfeld and two anonymous reviewers for constructive comments that greatly improved the quality of the manuscript.

References

Aloisi, G., Pierre, C., Rouchy, J.M., Foucher, J.P., Woodside, J., 2000. Methane-related authigenic carbonates of Eastern Mediterranean Sea mud volcanoes and their possible relation to gas hydrate destabilisation. Earth Planet. Sci. Lett. 184, 321–338. doi:10.1016/S0012-821X(00)00322-8

Ambrose, W. G. Jr., G. Panieri, A. Schneider, A. Plaza-Faverola, M. L. Carroll, E. K. L. Aström, W. L. Locke V, Carroll, J. 2015. Bivalve shell horizons in seafloor pockmarks of the last glacial interglacial transition: a thousand years of methane emissions in the Arctic Ocean, Geochem. Geophys. Geosyst., 16, 4108–4129, doi:10.1002/2015GC005980.

Bayon, G., Pierre, C., Etoubleau, J., Voisset, M., Cauquil, E., Marsset, T., Sultan, N., Le Drezen, E., Fouquet, Y., 2007. Sr/Ca and Mg/Ca ratios in Niger Delta sediments: Implications for authigenic carbonate genesis in cold seep environments. Mar. Geol. 241, 93–109. doi:10.1016/j.margeo.2007.03.007

Bentov, S., Erez, J., 2006. Impact of biomineralization processes on the Mg content of foraminiferal shells: A biological perspective. Geochemistry, Geophys. Geosystems 7. doi:10.1029/2005GC001015

515 Berndt, C., Feseker, T., Treude, T., Krastel, S., Liebetrau, V., Niemann, H., Bertics, V.J., Dumke, I.,
516 Dünnbier, K., Ferré, B., Graves, C., Gross, F., Hissmann, K., Hühnerbach, V., Krause, S., Lieser, K.,
517 Schauer, J., Steinle, L., 2014. Temporal Constraints on Hydrate-Controlled Methane Seepage off
518 Svalbard. Science (80-.). 343, 284–287. doi:10.1126/science.1246298

519 Blackmon, P.D., Todd, R., 1959. Paleontological Society Mineralogy of Some Foraminifera as Related
520 to Their Classification and Ecology Linked references are available on JSTOR for this article : J.
521 Paleontol. 33, 1–15.

522 Boetius, A, Ravenschlag, K., Schubert, C.J., Rickert, D., Widdel, F., Gieseke, a, Amann, R., Jørgensen,
523 B.B., Witte, U., Pfannkuche, O., 2000. A marine microbial consortium apparently mediating
524 anaerobic oxidation of methane. Nature 407, 623–626. doi:10.1038/35036572

525 Bohrmann, G., Greinert, J., Suess, E., Torres, M., 1998. Authigenic carbonates from the Cascadia
526 subduction zone and their relation to gas hydrate stability. Geology 26, 647–650.
527 doi:10.1130/0091-7613(1998)026<0647:ACFTCS>2.3.CO

528 Bond, G., Broecker, W., Johnsen, S., McManus, J., Labeyrie, L., J., J. & Bonani, G., 1993. Correlations
529 between climate records from North Atlantic sediments and Greenland ice. Nature 365, 143–
530 147.

531 Boyle, E.A., Rosenthal, Y., 1996. Chemical hydrography of the south Atlantic during the Last Glacial
532 Maximum: Cd vs. 13C. In: Wefer, G., et al. (Eds.), The South Atlantic: Present and Past
533 Circulation. Springer, New York, pp. 423–443.

534 Bowden, D.A., Rowden, A.A., Thurber, A.R., Baco, A.R., Levin, L.A., Smith, C.R., 2013. Cold Seep
535 Epifaunal Communities on the Hikurangi Margin, New Zealand: Composition, Succession, and
536 Vulnerability to Human Activities. PLoS One 8. doi:10.1371/journal.pone.0076869

537 Bünz, S., Polyanov, S., Vadakkepuliyambatta, S., Consolaro, C., Mienert, J., 2012. Active gas venting
538 through hydrate-bearing sediments on the Vestnesa Ridge, offshore W-Svalbard. Mar. Geol.
539 332-334, 189–197. doi:10.1016/j.margeo.2012.09.012

540 Callender, R., Powell, E.N., 2000. Long-term history of chemoautotrophic clam-dominated faunas of
541 petroleum seeps in the Northwestern Gulf of Mexico. Facies 43, 177–204.
542 doi:10.1007/BF02536990

543 Consolaro, C., Rasmussen, T.L., Panieri, G., Mienert, J., Bünz, S., Sztybor, K., 2015. Carbon isotope
544 ($\delta^{13}C$) excursions suggest times of major methane release during the last 14 kyr in Fram Strait,
545 the deep-water gateway to the Arctic. Clim. Past 11, 669–685. doi:10.5194/cp-11-669-2015

546 Crémière, A., Bayon, G., Ponzevera, E., Pierre, C., 2013. Paleo-environmental controls on cold seep
547 carbonate authigenesis in the Sea of Marmara. Earth Planet. Sci. Lett. 376, 200–211.
548 doi:10.1016/j.epsl.2013.06.029

549 Crémière, A., Lepland, A., Chand, S., Sahy, D., Kirsimäe, K., Bau, M., Whitehouse, M.J., Noble, S.R.,
550 Martma, T., Thorsnes, T., Brunstad, H., 2016. Fluid source and methane-related diagenetic
551 processes recorded in cold seep carbonates from the Alvheim channel, central North Sea.
552 Chem. Geol. 432, 16–33. doi:10.1016/j.chemgeo.2016.03.019

553 Crémière, A., Pierre, C., Blanc-Valleron, M.M., Zitter, T., Çağ atay, M.N., Henry, P., 2012. Methane-
554 derived authigenic carbonates along the North Anatolian fault system in the Sea of Marmara
555 (Turkey). Deep. Res. Part I Oceanogr. Res. Pap. 66, 114–130. doi:10.1016/j.dsr.2012.03.014

556 Deschamps, P., Durand, N., Bard, E., Hamelin, B., Camoin, G., Thomas, A.L., Henderson, G.M., Okuno,
557 J., Yokoyama, Y., 2012. Ice-sheet collapse and sea-level rise at the Bølling warming 14,600 years
558 ago. Nature 483, 559–564. doi:10.1038/nature10902

559 Donners, J., 2002. A shape-persistent polymeric crystallization template for CaCO3. J. Am. … 9700–
560 9701. doi:10.1021/ja0267573

561 Eiken, O. and Hinz, K., 1993. Contourites in the Fram Strait. Sedimentary. Geology 82, 15–32.

562 Edgar, K.M., Pälike, H., Wilson, P.A., 2013. Testing the impact of diagenesis on the δ18O and δ13C of
563 benthic foraminiferal calcite from a sediment burial depth transect in the equatorial Pacific.
564 Paleoceanography 28, 468–480. doi:10.1002/palo.20045

565 Fairbanks, R.G., Mortlock, R.A., Chiu, T., Cao, L., Kaplan, A., Guilderson, T.P., Fairbanks, T.W., Bloom,
566 A.L., Grootes, P.M., 2005. Radiocarbon calibration curve spanning 0 to 50 , 000 years BP based
567 on paired 230 Th / 234 U / 238 U and 14 C dates on pristine corals. Quat. Sci. Rev. 24, 1781–
568 1796. doi:10.1016/j.quascirev.2005.04.007

569 Formolo, M.J., Lyons, T.W., Zhang, C., Kelley, C., Sassen, R., Horita, J., Cole, D.R., 2004. Quantifying
570 carbon sources in the formation of authigenic carbonates at gas hydrate sites in the Gulf of
571 Mexico. Chem. Geol. 205, 253–264. doi:10.1016/j.chemgeo.2003.12.021

572 Greinert, J., Bohrmann, G., Suess, E., 2001. Gas hydrate-associated carbonates and methane-venting
573 at Hydrate Ridge: Classification, distribution, and origin of authigenic lithologies. Geophys.
574 Monogr. Ser. 124, 99–113. doi:10.1029/GM124p0099

575 Herguera, J.C., Paull, C.K., Perez, E., Peltzer, E., 2014. Limits to the sensitivity of living benthic
576 foraminifera to pore water carbon isotope anomalies in methane vent environments 273–289.
577 doi:10.1002/2013PA002457.Received

578 Hill, T.M., Kennett, J.P., Valentine, D.L., 2004. Isotopic evidence for the incorporation of methane-
579 derived carbon into foraminifera from modern methane seeps, Hydrate Ridge, Northeast
580 Pacific. Geochim. Cosmochim. Acta 68, 4619–4627. doi:10.1016/j.gca.2004.07.012

581 Hong, W.-L; Sauer, S.; Panieri, G.; Ambrose, W.; James, R.; Plaza-Faverola, A.; Schneider,
582 A. 2016. Removal of methane through hydrological, microbial, and geochemical processes in
583 the shallow sediments of pockmarks along eastern Vestnesa Ridge (Svalbard). Limnology and
584 Oceanography 61, 324 – 343. doi: 10.1002/lno.10299.

585 Howe, J. a., Shimmield, T.M., Harland, R., 2008. Late quaternary contourites and glaciomarine
586 sedimentation in the Fram Strait. Sedimentology 55, 179–200. doi:10.1111/j.1365-
587 3091.2007.00897.x

588 Hustoft, S., Bünz, S., Mienert, J., Chand, S., 2009. Gas hydrate reservoir and active methane-venting
589 province in sediments on < 20 Ma young oceanic crust in the Fram Strait, offshore NW-
590 Svalbard. Earth Planet. Sci. Lett. 284, 12–24. doi:10.1016/j.epsl.2009.03.038

591 Jessen, S.P., Rasmussen, T.L., Nielsen, T., Solheim, A., 2010. A new Late Weichselian and Holocene
592 marine chronology for the western Svalbard slope 30,000-0 cal years BP. Quat. Sci. Rev. 29,
593 1301–1312. doi:10.1016/j.quascirev.2010.02.020

594 Johnson, J.E., Mienert, J., Plaza-Faverola, A., Vadakkepuliyambatta, S., Knies, J., Bünz, S., Andreassen,
595 K., Ferré, B., 2015. Abiotic methane from ultraslow-spreading ridges can charge Arctic gas
596 hydrates. Geology 43, 371–374. doi:10.1130/G36440.1

597 Judd, A.G., Hovland, M., 2007. Seabed Fluid Flow - The impact on Geology, Biology and the Marine
598 Environment. Cambridge University Press, Cambridge.

599 Kennett, J.P., Stott, L.D., 1991. Abrupt deep-sea warming, palaeoceanographic changes and benthic
600 extinctions at the end of the Palaeocene. Nature 353, 225–229. doi:10.1038/353225a0

601 Kiel, S. 2010. On the potential generality of depth-related ecologic structure in cold-seep

602 communities: Evidence from Cenozoic and Mesozoic examples. *Palaeogeography,*
603 *Palaeoclimatology, Palaeoecology*, *295*(1-2), 245–257.
604 http://doi.org/10.1016/j.palaeo.2010.05.042

605 Krylova, E.M., Sahling, H., 2010. Vesicomyidae (Bivalvia): Current taxonomy and distribution. PLoS
606 One 5. doi:10.1371/journal.pone.0009957

607 Levin, L.A., Baco, A.R., Bowden, D.A., Colaco, A., Cordes, E.E., Cunha, M.R., Demopoulos, A.W.J.,
608 Gobin, J., Grupe, B.M., Le, J., Metaxas, A., Netburn, A.N., Rouse, G.W., Thurber, A.R., Tunnicliffe,
609 V., Van Dover, C.L., Vanreusel, A., Watling, L., 2016. Hydrothermal Vents and Methane Seeps:
610 Rethinking the Sphere of Influence. Front. Mar. Sci. 3, 1–23. doi:10.3389/fmars.2016.00072

611 Lucchi, 2015. Marine sedimentary record of Meltwater Pulse 1a along the NW Barents Sea
612 continental margin. doi:10.1007/s41063-015-0008-6

613 Mackensen, A., Wollenburg, J., Licari, L., 2006. Low d13C in tests of live epibenthic and endobenthic
614 foraminifera at a site of active methane seepage. Paleoceanography 21, 1–12.
615 doi:10.1029/2005PA001196

616 Martin, R. a., Nesbitt, E. a., Campbell, K. a., 2010. The effects of anaerobic methane oxidation on
617 benthic foraminiferal assemblages and stable isotopes on the Hikurangi Margin of eastern New
618 Zealand. Mar. Geol. 272, 270–284. doi:10.1016/j.margeo.2009.03.024

619 Martin, R. a., Nesbitt, E. a., Campbell, K. a., 2007. Carbon stable isotopic composition of benthic
620 foraminifera from Pliocene cold methane seeps, Cascadia accretionary margin. Palaeogeogr.
621 Palaeoclimatol. Palaeoecol. 246, 260–277. doi:10.1016/j.palaeo.2006.10.002

622 Mattingsdal, R., Knies, J., Andreassen, K., Fabian, K., Husum, K., Grøsfjeld, K., De Schepper, S., 2014. A
623 new 6 Myr stratigraphic framework for the Atlantic–Arctic Gateway. Quat. Sci. Rev. 92, 170–
624 178. doi:10.1016/j.quascirev.2013.08.022

625 Mazzini, A., Ivanov, M.K., Parnell, J., Stadnitskaia, A., Cronin, B.T., Poludetkina, E., Mazurenko, L., Van
626 Weering, T.C.E., 2004. Methane-related authigenic carbonates from the Black Sea: Geochemical
627 characterisation and relation to seeping fluids. Mar. Geol. 212, 153–181.
628 doi:10.1016/j.margeo.2004.08.001

629 Millo, C., Sarnthein, M., Erlenkeuser, H., Grootes, P.M., Andersen, N., 2005. Methane-induced early
630 diagenesis of foraminiferal tests in the southwestern Greenland Sea. Mar. Micropaleontol. 58,
631 1–12. doi:10.1016/j.marmicro.2005.07.003

632 Mienert, J. 2013. CAGE Cruise Report for 08 October 2013–25 October 2013 on Board the FF Helmer
633 Hanssen, 42 pp., The Arctic University of Tromsø, Tromsø, Norway.

634 Naehr, T.H., Eichhubl, P., Orphan, V.J., Hovland, M., Paull, C.K., Ussler, W., Lorenson, T.D., Greene,
635 H.G., 2007. Authigenic carbonate formation at hydrocarbon seeps in continental margin
636 sediments: A comparative study. Deep. Res. Part II Top. Stud. Oceanogr. 54, 1268–1291.
637 doi:10.1016/j.dsr2.2007.04.010

638 Panieri, G., 2006. Foraminiferal response to an active methane seep environment: A case study from
639 the Adriatic Sea. Mar. Micropaleontol. 61, 116–130. doi:10.1016/j.marmicro.2006.05.008

640 Panieri, G., A. Camerlenghi, S. Conti, G. A. Pini, and I. Cacho (2009), Methane seepages recorded in
641 benthonic foraminifera from Miocene seep carbonates, Northern Apennines (Italy),
642 Palaeogeogr. Palaeoclimatol. Palaeoecol., 284, 271–282.

643 Panieri, G., James, R.H., Camerlenghi, A., Cesari, V., Cervera, C.S., Cacho, I., Westbrook, G.K., 2014.

644 Record of methane emissions from the West Svalbard continental margin during the last 16 ,
645 000 years revealed by δ 13 C of benthic foraminifera . Glob. Planet. Change 122, 151–160.
646 doi:10.1016/j.gloplacha.2014.08.014

647 Panieri, G., Graves, C. A., James, R. H. 2016a. Paleo-methane emissions recorded in foraminifera near
648 the landward limit of the gas hydrate stability zone offshore western Svalbard, Geochem.
649 Geophys. Geosyst., 17, doi:10.1002/2015GC006153.

650 Panieri, G., Lepland, A., Whitehouse, M. J., Wirth, R., Raanes, M. P., James, R. H., Graves, C. A.,
651 Crémière. A., Schneider, A. 2016b. Diagenetic Mg-calcite overgrowths on foraminiferal tests in
652 the vicinity of methane seeps. Earth and Planetary Science Letters 458, 203-212,
653 http://dx.doi.org/10.1016/j.epsl.2016.10.024. Panieri, G., Sen Gupta, B.K., 2008. Benthic
654 Foraminifera of the Blake Ridge hydrate mound, Western North Atlantic Ocean. Mar.
655 Micropaleontol. 66, 91–102. doi:10.1016/j.marmicro.2007.08.002

656 Pena, L.D., Calvo, E., Cacho, I., Eggins, S., Pelejero, C., 2005. Identification and removal of Mn-Mg-rich
657 contaminant phases on foraminiferal tests: Implications for Mg/Ca past temperature
658 reconstructions. Geochemistry, Geophys. Geosystems 6. doi:10.1029/2005GC000930

659 Petersen, C.J., Bünz, S., Hustoft, S., Mienert, J., Klaeschen, D., 2010. High-resolution P-Cable 3D
660 seismic imaging of gas chimney structures in gas hydrated sediments of an Arctic sediment drift.
661 Mar. Pet. Geol. 27, 1981–1994. doi:10.1016/j.marpetgeo.2010.06.006

662 Plaza-Faverola, a., Bünz, S., Johnson, J.E., Chand, S., Knies, J., Mienert, J., Franek, P., 2015. Role of
663 tectonic stress in seepage evolution along the gas hydrate-charged Vestnesa Ridge, Fram Strait.
664 Geophys. Res. Lett. 42, 733–742. doi:10.1002/2014GL062474

665 Rathburn, a E., Levin, L. a, Held, Z., Lohmann, K.C., 2000. Benthic foraminifera associated with cold
666 seeps on the northern California margin: Ecology and stableisotopic composition. Mar.
667 Micropaleontol. 38, 247–266.

668 Rathburn, A.E., Elena P??rez, M., Martin, J.B., Day, S.A., Mahn, C., Gieskes, J., Ziebis, W., Williams, D.,
669 Bahls, A., 2003. Relationships between the distribution and stable isotopic composition of living
670 benthic foraminifera and cold methane seep biogeochemistry in Monterey Bay, California.
671 Geochemistry, Geophys. Geosystems 4. doi:10.1029/2003GC000595

672 Regenberg, M., Nürnberg, D., Schönfeld, J., Reichart, G.-J., 2007. Early diagenetic overprint in
673 Caribbean sediment cores and its effect on the geochemical composition of planktonic
674 foraminifera. Biogeosciences Discuss. 4, 2179–2213. doi:10.5194/bgd-4-2179-2007

675 Reimer, P.J., Bard, E., Bayliss, A., Beck, J.W., Blackwell, P.G., Bronk, C., Caitlin, R., Hai, E.B., Edwards,
676 R.L., 2013. Intcal13 and marine13 radiocarbon age calibration curves 0 – 50,000 years cal bp.
677 Radiocarbon 55, 1869–1887.

678 Richter, T.O., van der Gaast, S., Koster, B., Vaars, a., Gieles, R., de Stigter, H.C., De Haas, H., van
679 Weering, T.C.E., 2006. The Avaatech XRF Core Scanner: technical description and applications to
680 NE Atlantic sediments. Geol. Soc. London, Spec. Publ. 267, 39–50.
681 doi:10.1144/GSL.SP.2006.267.01.03

682 Sahling, H., Rickert, D., Lee, R.W., Linke, P., Suess, E., 2002. Macrofaunal community structure and
683 sulfide flux at gas hydrate deposits from the Cascadia convergent margin, NE Pacific. Mar. Ecol.
684 Prog. Ser. 231, 121–138. doi:10.3354/meps231121

685 Seidenkrantz, M.-S. 1995. Cassidulina teretis Tappan and Cassidulina neoteretis new species
686 (Foraminifera): stratigraphic markers for deep sea and outer shelf areas. Journal of
687 Micropalaeontology 14, 145–157.

688 Sen Gupta B. K., Platon E., Bernhard J. M., and Ahron P. (1997) Foraminiferal colonization of
689 hydrocarbon-seep bacterial mats and underlying sediment, Gulf of Mexico Slope. Journal of
690 Foraminiferal Research 27 (4), pp. 292–300.

691 Sexton, P.F., Wilson, P.A., 2009. Preservation of benthic foraminifera and reliability of deep-sea
692 temperature records: Importance of sedimentation rates, lithology, and the need to examine
693 test wall structure. Paleoceanography 24. doi:10.1029/2008PA001650

694 Sexton, P.F., Wilson, P.A., Pearson, P.N., 2006. Microstructural and geochemical perspectives on
695 planktic foraminiferal preservation: "glassy" versus "frosty." Geochemistry, Geophys.
696 Geosystems 7. doi:10.1029/2006GC001291

697 Smith, A.J., Mienert, J., Bünz, S., Greinert, J., Rasmussen, T.L., 2014. 900-m high gas plumes rising
698 from marine sediments containing structure II hydrates at Vestnesa Ridge , offshore W-Svalbard
699 15, 9302. doi:10.1029/2005JC003183.Vogt

700 Stakes, D.S., Orange, D., Paduan, J.B., Salamy, K. a., Maher, N., 1999. Cold-seeps and authigenic
701 carbonate formation in Monterey Bay, California. Mar. Geol. 159, 93–109. doi:10.1016/S0025-
702 3227(98)00200-X

703 Stott, L.D., 2002. Does the oxidation of methane leave an isotopic fingerprint in the geologic record?
704 Geochemistry Geophys. Geosystems 3, 1–16. doi:10.1029/2001GC000196

705 Stuiver, M., P. J. Reimer, and R. Reimer (2014), CALIB Radiocarbon Calibration Execute, Version
706 7.0html. [Available at http://calib.qub.ac.uk/calib/.]

707 Sztybor, K., Rasmussen, T.L., 2016. Diagenetic disturbances of marine sedimentary records from
708 methane-influenced environments in the Fram Strait as indications of variation in seep intensity
709 during the last 35 000 years. Boreas. doi:10.1111/bor.12202

710 Thomas, E., 2002. Warming the Fuel for the Fire : Evidence for the Thermal Dissociation of Methane
711 Hydrate During the Paleocene-Eocene Thermal Maximum dissociation of methane hydrate
712 during the Paleocene-Eocene 1–5. doi:10.1130/0091-7613(2002)030<1067:WTFFTF>2.0.CO;2

713 Torres, M. E., McManus, J. , Hammond, D. E. , de Angelis, M. A., Heeschen, K. U., Colbert, S. L., Tryon,
714 M. D., Brown, K. M., Suess, E. 2002. Fluid and chemical fluxes in and out of sediments hosting
715 methane hydrate deposits on Hydrate Ridge, OR, I: Hydrological provinces. Earth and Planetary
716 Science Letters 201, 525–540. doi: 10.1016/S0012-821X(02)00733-1

717 Torres, M.E., 2003. Is methane venting at the seafloor recorded by D13C of benthic foraminifera
718 shells? Paleoceanography 18, 1–13. doi:10.1029/2002PA000824

719 Torres, M.E., Martin, R. a., Klinkhammer, G.P., Nesbitt, E. a., 2010. Post depositional alteration of
720 foraminiferal shells in cold seep settings: New insights from flow-through time-resolved
721 analyses of biogenic and inorganic seep carbonates. Earth Planet. Sci. Lett. 299, 10–22.
722 doi:10.1016/j.epsl.2010.07.048

723 Taylor, J. D., and E. A. Glover 2010. Chemosynthetic bivalves, in The Vent and Seep Biota, Top.
724 Geobiol., vol. 33, edited by S. Kiel, pp. 107–155, Springer Science and Bussiness Media B.V.,
725 Berlin, Germany.

726 Vogt, P.R., Crane, K., Sundvor, E., Max, M.D., Pfirman, S.L., 1994. Methane-generated(?) pockmarks
727 on young, thickly sedimented oceanic crust in the Arctic: Vestnesa Ridge, Fram Strait. Geology
728 22, 255–258. doi:10.1130/0091-7613(1994)022<0255:MGPOYT>2.3.CO;2

729 Winkelmann, D., Geissler, W., Schneider, J., Stein, R., 2008. Dynamics and timing of the
730 Hinlopen/Yermak Megaslide north of Spitsbergen, Arctic Ocean. Mar. Geol. 250, 34–50.

731 doi:10.1016/j.margeo.2007.11.013

732 Wefer, G., P.-M. Heinze, Berger, W. H. 1994. Clues to ancient methane release, Nature, 369, 282,
733 1994.

734 Wollenburg, J.E., Raitzsch, M., Tiedemann, R., 2015. Novel high-pressure culture experiments on
735 deep-sea benthic foraminifera - Evidence for methane seepage-related δ13C of Cibicides
736 wuellerstorfi. Mar. Micropaleontol. 117, 47–64. doi:10.1016/j.marmicro.2015.04.003

737 Wollenburg, J.E., Kuhnt, W., Mackensen, A., 2001. Changes in Arctic Ocean paleoproductivity and
738 hydrography during the last 145 kyr: the benthic foraminiferal record. Paleoceanography 16,
739 65–77.

Figure captions

Figure 1
Map of study area. **(A)** Bathymetric map of the west Svalbard margin and east Fram Strait. The red box indicates the location of the investigated area at Vestnesa Ridge. MFZ - Molloy Fracture Zone. MD - Molloy Deep. MR - Molloy Ridge. SFZ - Spitsbergen Fracture Zone. **(B)** Swath bathymetry map of Vestnesa Ridge with the location of the studied core HH-13-203 (black circle). For areas shaded in grey, high-resolution swath bathymetric data are not available. Figure modified from Hustoft et al. (2009).

Figure 2
(A) Lithological description and geochemical records of benthic foraminifera and carbonate nodules in gravity core HH-13-203. Regional chronological framework from the western Svalbard continental margin published by Jessen et al. (2010) using ages calibrated according to Fairbanks et al. (2005). Ages adopted from Ambrose et al. (2015) were calibrated using the Calib 7.1 program (Stuiver et al., 2014) and the marine calibration curve Marine 13 (Reimer et al., 2013). Present-day Sulphate-Methane Transition Zone (SMTZ) after Hong et al. (2016). Normal range of $\delta^{13}C$ in benthic foraminifera from 0 to -1 ‰ after Wollenburg et al. (2001). Note varying scales and breaks in the horizontal axes for $\delta^{13}C$ and $\delta^{18}O$. **(B)** Paleo-environmental interpretation. CBC - Chemosynthetic bivalve community. EH - Early Holocene. HE 1 - Heinrich Event 1. LGM - Last Glacial Maximum.

Figure 3
Backscattered SEM photomicrographs of exposed surfaces after crushing the carbonate nodules in HH-13-203, 220 to 250 cm. **(A)** Microcrystalline high-Mg calcite with disseminated pyrite (white dots). **(B)** Cavities between high-Mg calcite create porosity in the carbonate nodules. **(C; D)** Detrital silica grain embedded in microcrystalline high-Mg calcite. Scale bars are 20 µm.

Figure 4
Pristine *C. neoteretis* tests and tests exhibiting minor, moderate and major diagenetic alteration (DA). **(A)** View using a light microscope, **(B)** Backscatter-SEM image exterior wall, **(C)** Backscatter-SEM image interior wall, **(D)** correspondent EDS image. The colour-change from green in pristine tests towards a yellow-orange hue in diagenetically altered tests reflects a change in Mg-content from low (green) to high (yellow-orange). Detail of the image shown in (D) as Backscatter-SEM image **(E)** and EDS map **(F)**. We rotated images E and F for moderate and major diagenetic alteration by 90° anticlockwise. Scale in A to D is 100 µm, scale bars in E and F are 20 µm.

Figure 5
Guide to test microstructural characteristics of *C. neoteretis* and classification of diagenetic alteration (DA). Whole tests are imaged for exterior wall view, polished sections for interior wall view and high-Mg calcite maps. Pristine "glassy" foraminifera tests were found in stratigraphic intervals that were deposited in a normal marine environment lacking the influence of methane-charged pore fluids. In contrast, less well preserved "frosty" foraminifera experienced diagenetic alteration due to the precipitation of methane-derived authigenic carbonate after burial. LM – light microscopy, SEM – backscatter scanning electron microscopy, EDS - energy dispersive X-ray spectrometry.

Figure 6
Cross-plot of $\delta^{13}C$ and $\delta^{18}O$ values obtained from unaltered tests of the benthic foraminifera species *C. neoteretis* (C. n.) (cluster A), diagenetically altered foraminifera tests inside and outside the shell bed (cluster B), and carbonate nodules (cluster C). Normal range of $\delta^{13}C$ in benthic foraminifera from 0 to -1 ‰ according to Wollenburg et al. (2001).

Figure 7
Backscatter-SEM images showing interior wall microstructure and aspect of pores in different stages of diagenetic alteration (DA) in *C. neoteretis*. **(A)** Optically smooth pristine test with unplugged pores. **(B)** Interior wall with rare high-Mg calcite crystals. **(C)** Dense high-Mg calcite crystals on interior wall while pores remain unplugged. **(D)** Pores still unplugged, but immediate vicinity is overgrown with high-Mg calcite crystals. **(E)** Detail of (D) with authigenic carbonate crystals and pores. **(F)** High-Mg calcite crystals forming a thick coating inside a chamber, pores are invisible. Scale bars are 10 µm.

Table captions

Table 1
Carbon and oxygen stable isotopic composition of benthic foraminifera calcite tests and carbonate nodules recovered from gravity core HH-13-203. Sections shaded in light grey correspond to identified methane seepage episodes during HE1 with diagenetic alteration of foraminifera (Fig. 2), sections shaded in dark grey correspond to the stratigraphic extent of the shell bed according to Ambrose et al. (2015).

Figures

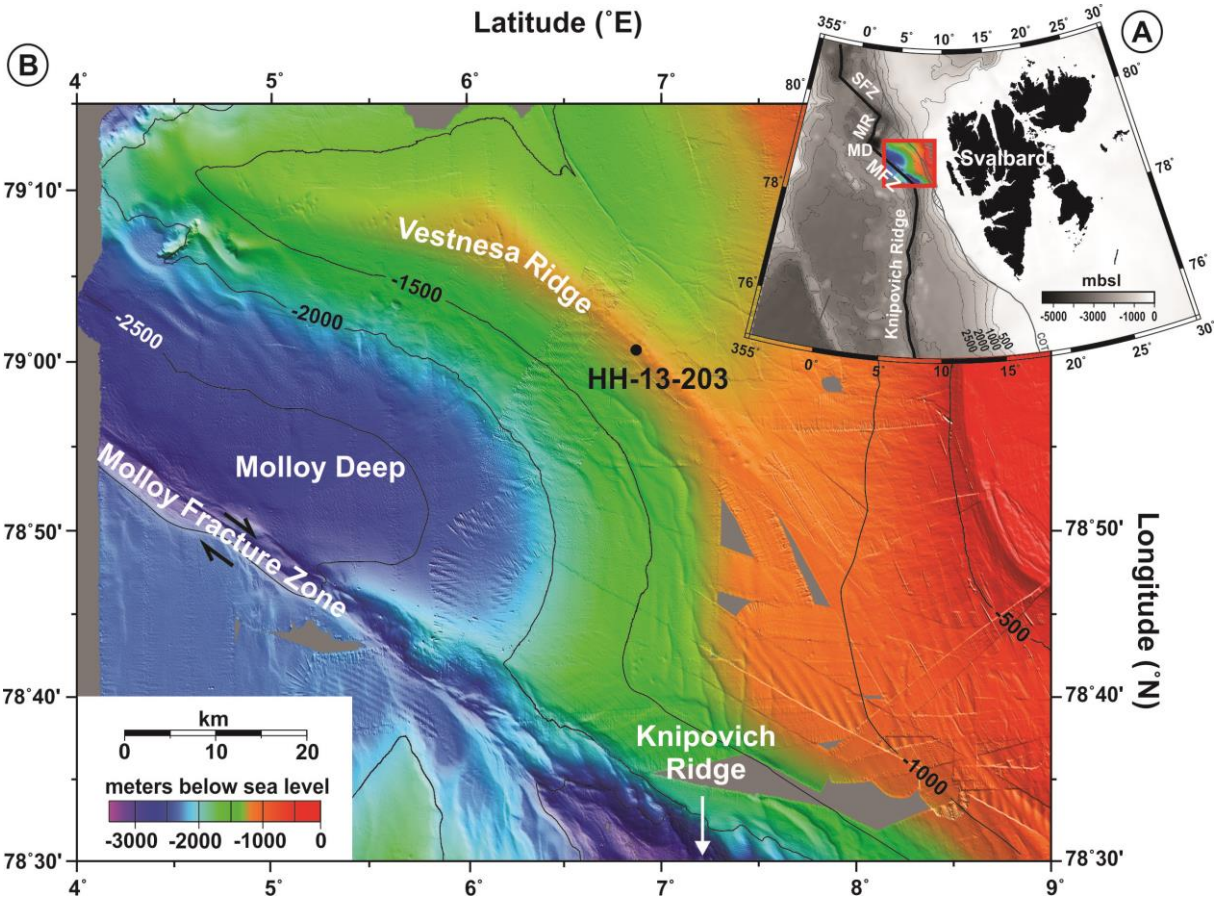

Figure 1

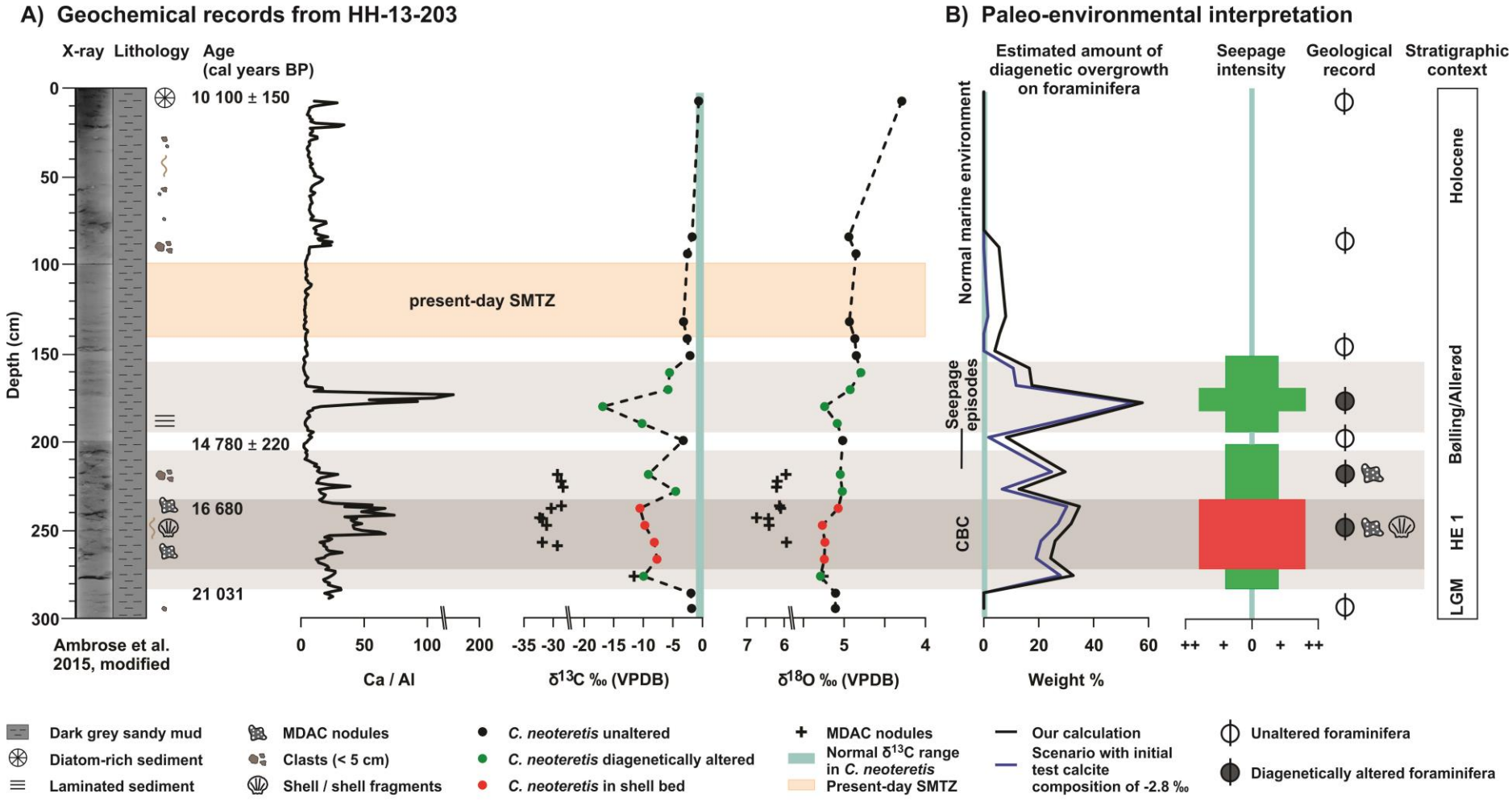
A) Geochemical records from HH-13-203
X-ray
Lithology
Age (cal years BP)
10 100 ± 150
14 780 ± 220
16 680
21 031
Depth (cm)
present-day SMTZ
Ambrose et al. 2015, modified
Ca / Al
δ13C ‰ (VPDB)
δ18O ‰ (VPDB)
B) Paleo-environmental interpretation
Estimated amount of diagenetic overgrowth on foraminifera
Normal marine environment
Seepage episodes
CBC
Weight %
Seepage intensity
Geological record
Stratigraphic context
Holocene
Bølling/Allerød
HE 1
LGM
Dark grey sandy mud
Diatom-rich sediment
Laminated sediment
MDAC nodules
Clasts (< 5 cm)
Shell / shell fragments
C. neoteretis unaltered
C. neoteretis diagenetically altered
C. neoteretis in shell bed
MDAC nodules
Normal δ13C range in C. neoteretis
Present-day SMTZ
Our calculation
Scenario with initial test calcite composition of -2.8 ‰
Unaltered foraminifera
Diagenetically altered foraminifera

Figure 2

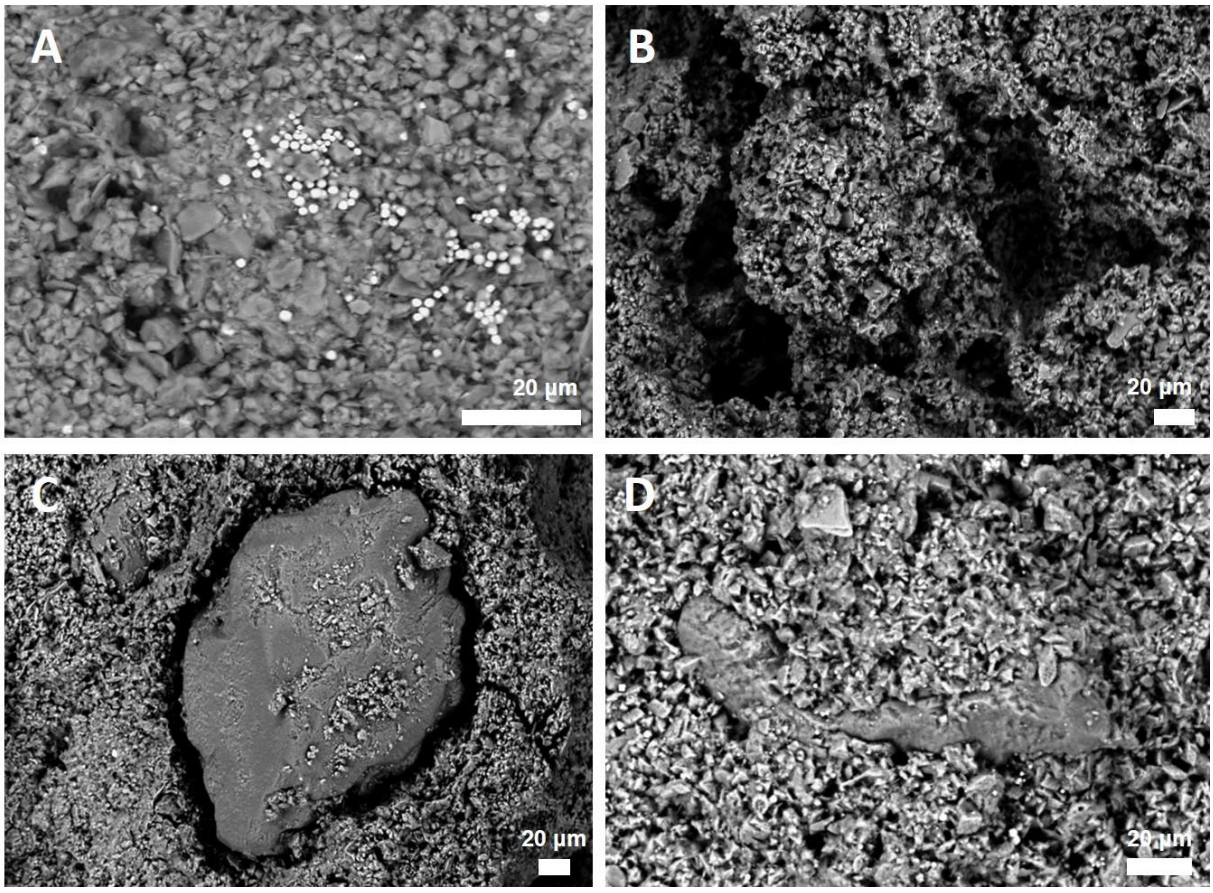

Figure 3

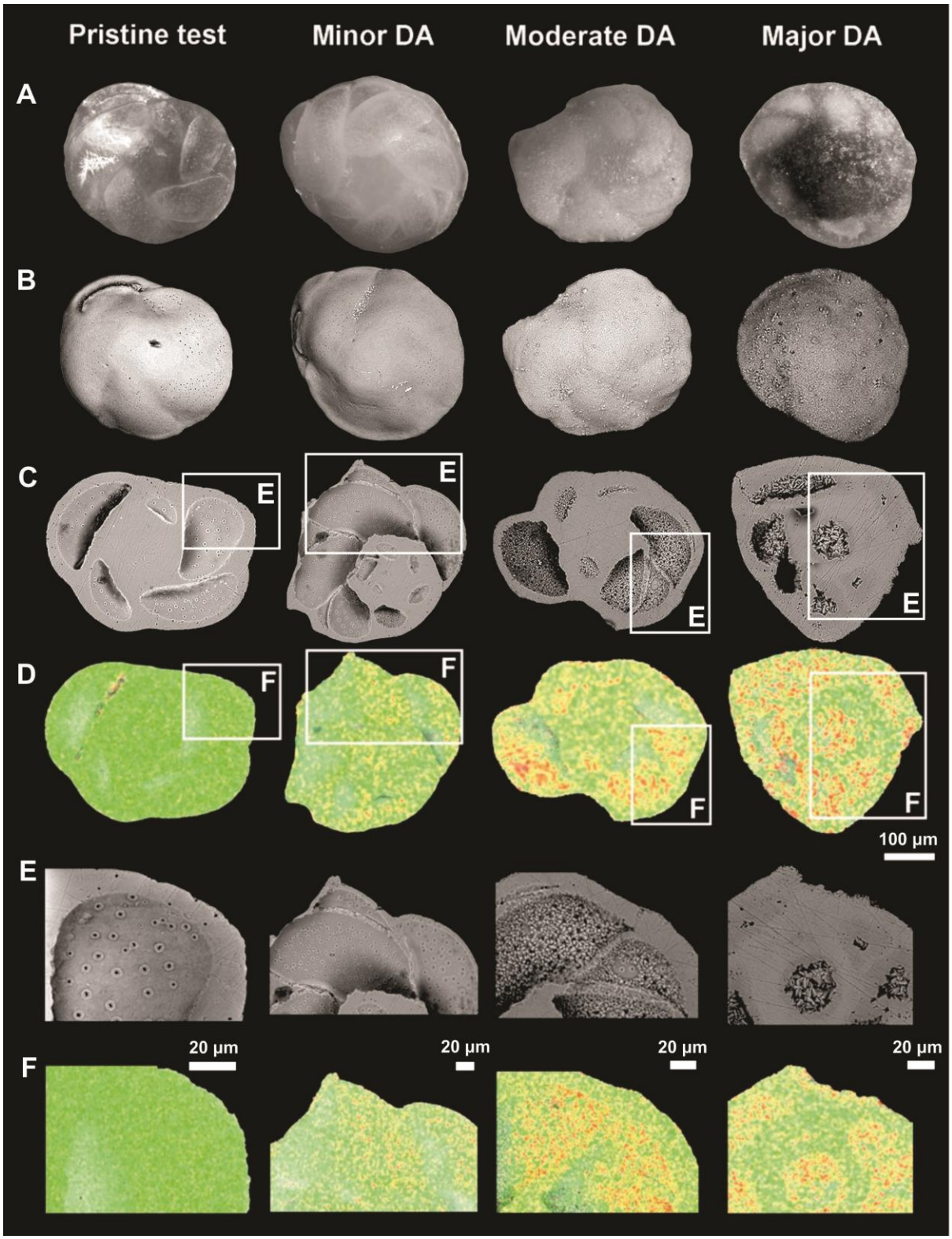
Pristine test
Minor DA
Moderate DA
Major DA
A
B
C
D
E
F
E
F
100 µm
20 µm
20 µm
20 µm
20 µm

Figure 4

Pristine test	Minor DA	Moderate DA	Major DA

Exterior Wall (LM)

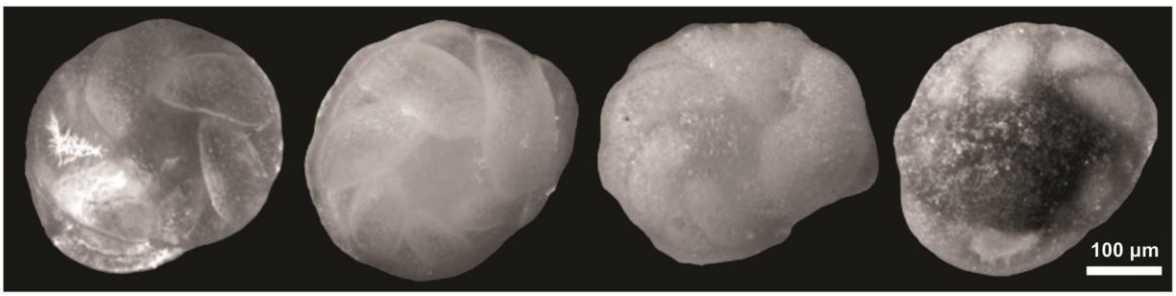

Surface	"Glassy"	"Glassy"	"Frosty"	"Frosty"
Reflectance	High	Low	Low	Low
Transparency	Yes	Yes/No	No	No
Colour	Translucent, light grey	Translucent, white	white to yellow	yellow to dark brown
Ornamentation	Visible	Visible	Invisible	Invisible

Interior Wall (SEM)

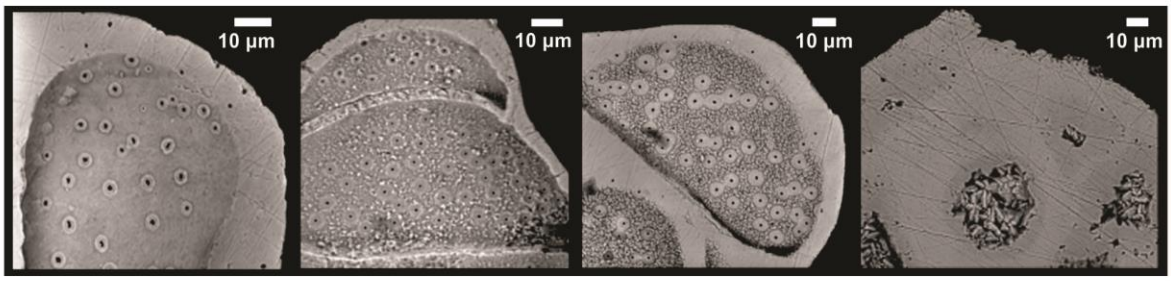

Foreign grains or crystals absent	Rare high-Mg calcite crystals	Pervasive high-Mg calcite crystals	Well-developed high-Mg calcite crystals covering the specimen

High-Mg Calcite crystals (EDS)

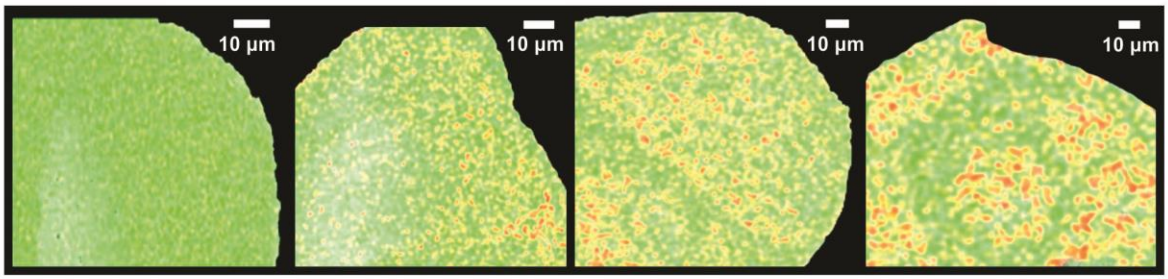

Absent	Present, forming single crystals	Present, dense crystal cover	Present, forming solid crust

Mg-content

Figure 5

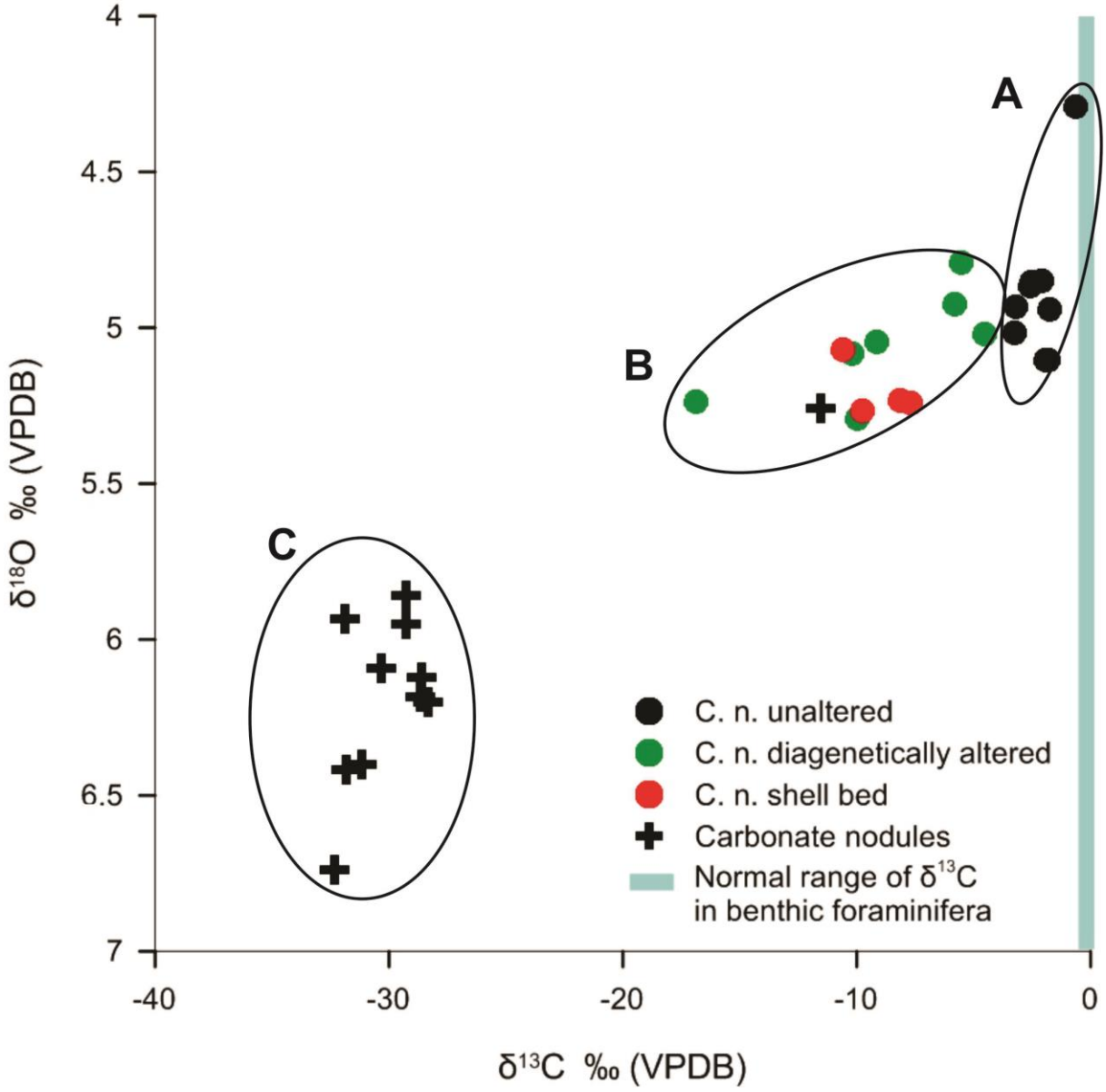
A
B
C
C. n. unaltered
C. n. diagenetically altered
C. n. shell bed
Carbonate nodules
Normal range of δ13C
in benthic foraminifera
δ18O ‰ (VPDB)
δ13C ‰ (VPDB)
4
4.5
5
5.5
6
6.5
7
-40
-30
-20
-10
0

Figure 6

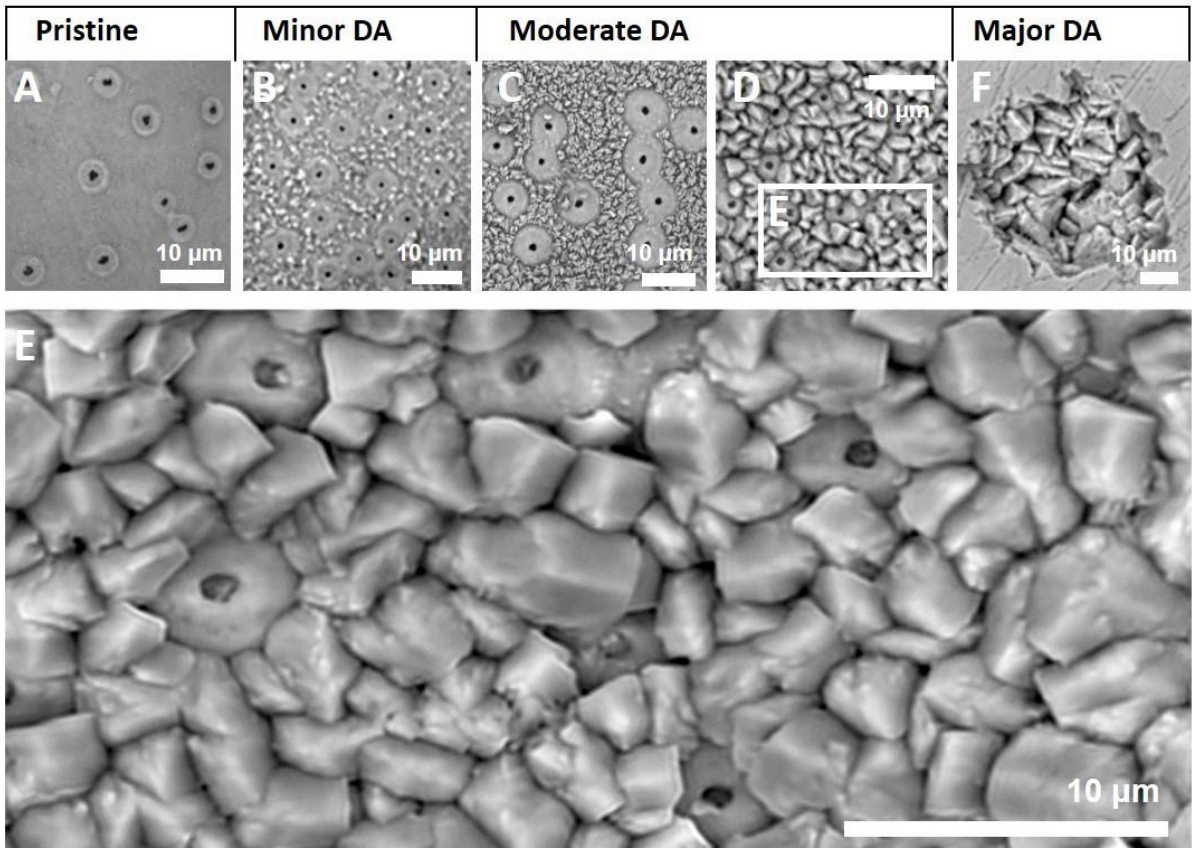
Pristine
Minor DA
Moderate DA
Major DA
A
B
C
D
E
F
10 µm
10 µm
10 µm
10 µm
10 µm
E
10 µm

Figure 7

Table 1

Depth beneath surface (cm)	*Cassidulina neoteretis* $\delta^{13}C$ (‰ VPDB)	*Cassidulina neoteretis* $\delta^{18}O$ (‰ VPDB)	Carbonate nodules $\delta^{13}C$ (‰ VPDB)	Carbonate nodules $\delta^{18}O$ (‰ VPDB)	Authigenic contribution (weight %)
0.5	-0.63	4.29			-
80.5	-1.74	4.94			-
90.5	-2.52	4.85			0-6
130.5	-3.19	4.93			2-8
140.5	-2.58	4.87			0-6
150.5	-2.10	4.85			0-4
160.5	-5.55	4.79			11-17
170.5	-5.82	4.92			12-18
180.5	-16.86	5.24			55-58
190.5	-10.22	5.08			29-34
200.5	-3.25	5.02			2-8
220.5	-9.14	5.05	-29.27	5.95	25-30
224.5			-28.65	6.18	-
228			-28.31	6.20	-
230.5	-4.52	5.02			7-13
239			-28.59	6.12	-
240.5	-10.57	5.07	-30.34	6.09	30-35
246			-32.30	6.74	-
246.5			-31.81	6.42	-
250.5	-9.74	5.27	-31.13	6.40	27-32
260.5	-8.13	5.24	-31.86	5.94	21-26
262.5			-29.29	5.86	-
270.5	-7.69	5.24			19-24
280.5	-9.95	5.29	-11.55	5.26	28-33
290.5	-1.94	5.10			-
299.5	-1.82	5.11			-